



# Performance improvement of amorphous Ga<sub>2</sub>O<sub>3</sub> ultraviolet photodetector by annealing under oxygen atmosphere

Changqi Zhou <sup>a,b</sup>, Kewei Liu <sup>a,b,\*</sup>, Xing Chen <sup>a</sup>, Jiaheng Feng <sup>c</sup>, Jialin Yang <sup>a</sup>, Zhenzhong Zhang <sup>a,b</sup>, Lei Liu <sup>a,b</sup>, Yang Xia <sup>d,e</sup>, Dezhen Shen <sup>a,b,\*\*</sup>

<sup>a</sup> State Key Laboratory of Luminescence and Applications, Changchun Institute of Optics, Fine Mechanics and Physics, Chinese Academy of Sciences, Changchun, 130033, China

<sup>b</sup> Center of Materials Science and Optoelectronics Engineering, University of Chinese Academy of Sciences, Beijing, 100049, China

<sup>c</sup> Jiaxing Research and Commercialization Center for Microelectronics Equipment, Chinese Academy of Sciences, Jiaxing, 314022, China

<sup>d</sup> Institute of Microelectronics of Chinese Academy of Sciences, Beijing, 100029, China

<sup>e</sup> University of Chinese Academy of Sciences, Beijing, 100049, China



## ARTICLE INFO

### Article history:

Received 25 December 2019

Received in revised form

9 May 2020

Accepted 9 May 2020

Available online 24 May 2020

### Keywords:

Amorphous Ga<sub>2</sub>O<sub>3</sub>

Solar-blind UV detector

Rejection ratio

Annealing under oxygen atmosphere

## ABSTRACT

We have demonstrated the fast-speed and high-rejection-ratio solar-blind ultraviolet (UV) photodetectors based on amorphous Ga<sub>2</sub>O<sub>3</sub> (a-Ga<sub>2</sub>O<sub>3</sub>) films grown by atomic layer deposition. The effect of the annealing under oxygen atmosphere on the performance of a-Ga<sub>2</sub>O<sub>3</sub> photodetectors is investigated. By the oxygen annealing at 500 °C, the 90–10% decay time of a-Ga<sub>2</sub>O<sub>3</sub> photodetector can be decreased to ~150 ns, and the UV/Visible rejection ratio of the photodetector can reach as high as  $2.74 \times 10^5$ , due to the significant suppression of the visible light response. Moreover, the dark current of the 500 °C-annealed photodetector is only 9.43 pA at 10 V bias. These phenomena can be explained by the decrease in oxygen vacancy concentration of the a-Ga<sub>2</sub>O<sub>3</sub> films after the oxygen annealing. The combination of high rejection ratios and fast operating speeds offers a viable way for facile and scalable fabrication of the oxide semiconductor solar-blind UV detectors.

© 2020 Elsevier B.V. All rights reserved.

## 1. Introduction

Owing to the advantages of high selectivity and strong anti-interference ability, the solar-blind ultraviolet (UV) photodetectors have a wide range of applications, such as flame detection, missile warning system and confidential communication [1–7]. The solar-blind UV photodetectors based on wide-bandgap semiconductor materials including diamond, AlGaN, ZnMgO and Ga<sub>2</sub>O<sub>3</sub>, have attracted the increasing attention due to their small size, all solid-state, intrinsic solar-blind, high radiation hardness and so on [8–13]. Compared with other wide-bandgap semiconductor materials, Ga<sub>2</sub>O<sub>3</sub> possesses suitable bandgap of 4.5 eV–4.9 eV, which is ideal for solar-blind detection without any additional alloying

process [14–16]. As the most stable phase of Ga<sub>2</sub>O<sub>3</sub>, β-Ga<sub>2</sub>O<sub>3</sub> has been widely used to fabricate the solar-blind photodetectors [17–25]. For example, Shen *et al.* [20] have prepared β-Ga<sub>2</sub>O<sub>3</sub> photodetectors with different thicknesses and the effect of thickness on the device performance has been investigated. Yu *et al.* [21] have reported β-Ga<sub>2</sub>O<sub>3</sub>/4H-SiC photodetector with a rise time of 11 ms and a decay time of 19 ms at 0 V. The metal-semiconductor-metal (MSM) β-Ga<sub>2</sub>O<sub>3</sub> photodetector with a large rejection ratio R<sub>254/365nm</sub> of  $>10^7$  and a high responsivity of 46 A/W have also been reported by Qiao *et al.* [25]. However, the preparation of high-quality β-Ga<sub>2</sub>O<sub>3</sub> film generally requires ultra-high-vacuum epitaxy techniques, including molecular beam epitaxy (MBE), metal-organic chemical vapor deposition (MOCVD), and pulsed laser deposition (PLD), which increases the costs and hinders its large-scale practical applications [17,18,20–25]. In addition, to achieve high-quality films, lattice matching substrates and high growth temperature are also required. With the development of flexible optoelectronic devices and large-area photovoltaic devices, there is an urgent need for materials with low cost, simple preparation process, large-area production, and low preparation

\* Corresponding author. State Key Laboratory of Luminescence and Applications, Changchun Institute of Optics, Fine Mechanics and Physics, Chinese Academy of Sciences, Changchun, 130033, China.

\*\* Corresponding author. State Key Laboratory of Luminescence and Applications, Changchun Institute of Optics, Fine Mechanics and Physics, Chinese Academy of Sciences, Changchun, 130033, China.

E-mail addresses: liukw@ciomp.ac.cn (K. Liu), shendz@ciomp.ac.cn (D. Shen).

temperature. Therefore, more and more attention has been focused on the amorphous  $\text{Ga}_2\text{O}_3$  ( $\text{a-Ga}_2\text{O}_3$ ) due to its lower preparation technical requirement, lower growth temperature, no need for lattice matching substrate, easy to form large area and excellent photoelectric properties [26–30]. Till now, the research on  $\text{a-Ga}_2\text{O}_3$  photodetector has made a lot of progress, and various methods, including sputtering and atom layer deposition (ALD), have been used to fabricate the  $\text{a-Ga}_2\text{O}_3$  films and their solar-blind UV photodetectors with relative higher responsivity. Recently, Zhou *et al.* [31] and Han *et al.* [32] have fabricated the high-performance  $\text{a-Ga}_2\text{O}_3$  photodetectors with the responsivity of 1099 A/W and 436 A/W, respectively. Zhu *et al.* [33] have demonstrated the  $\text{a-Ga}_2\text{O}_3$  photodetectors using different growth-temperature, and the  $\text{a-Ga}_2\text{O}_3$  photodetector grown at 500 °C showed the responsivity of 138 A/W. However, the photodetectors based on  $\text{a-Ga}_2\text{O}_3$  films still suffer from the following problems: First, the response speed is far from the strict requirements of modern high-speed detection due to the persistent photoconductivity (PPC) effect caused by defects in  $\text{a-Ga}_2\text{O}_3$  film [26,29]. Second, the transition from the valence band tail state or other defect level to the conduction band may cause a response to the long-wavelength light, which may reduce the UV/Visible rejection ratio of detector and seriously reduce the ability to distinguish the signal from the noise [27,30,34,35]. By analyzing the previous reports, it can be found that the above mentioned problems are related to the oxygen vacancies ( $V_O$ ) in  $\text{a-Ga}_2\text{O}_3$  [28,36]. Although the oxygen vacancy concentration of the  $\text{a-Ga}_2\text{O}_3$  film could be reduced by adjusting the O-source-flow during growth, the response speed is still not very quick (more than tens of  $\mu\text{s}$ ) and it is often accompanied by a dramatically decrease in responsivity (more than two orders of magnitude).

In this work, the effect of post-annealing on the performance of  $\text{a-Ga}_2\text{O}_3$  film photodetectors has been investigated. The  $\text{a-Ga}_2\text{O}_3$  films were fabricated on sapphire substrates by ALD and then were annealed in oxygen atmosphere at different temperatures. When the annealing temperature is below 550 °C, the samples still remain amorphous. After the annealing, the response speed of the  $\text{a-Ga}_2\text{O}_3$  photodetectors could be improved and the 90–10% decay time decreased from 220 ns (as-grown) to 150 ns (500 °C annealing) with a decrease in responsivity from 28 A/W to 1.34 A/W. Interestingly, the rejection ratio of  $\text{a-Ga}_2\text{O}_3$  photodetector was enhanced from  $4.3 \times 10^3$  to  $2.74 \times 10^5$  after annealing at 500 °C. The findings in this work provide a viable way to achieve high performance  $\text{Ga}_2\text{O}_3$  solar-blind UV detectors for the requirements of effective detection and rapid response.

## 2. Experimental section

The  $\text{a-Ga}_2\text{O}_3$  films were grown on  $c\text{-Al}_2\text{O}_3$  substrates by ALD (Kemicro T-ALD150A) in a low vacuum condition of 0.2 torr with substrate temperature kept at 280 °C. The trimethylgallium (TMGa) and  $\text{O}_3/\text{H}_2\text{O}$  were used as a Ga-precursor and an oxygen source, respectively. The TMGa was kept at the temperature of –5 °C. First, TMGa precursor was injected into the reaction chamber for 18 ms followed by  $\text{N}_2$  (40 sccm) purging for 40 s. Next,  $\text{O}_3$  and  $\text{H}_2\text{O}$  were introduced into the chamber for 10 s and 15 ms, respectively, and then the chamber was purged with  $\text{N}_2$  (40 sccm) for 40 s. The entire growth time of  $\text{a-Ga}_2\text{O}_3$  films was 50 h. After that, the as-grown films were annealed in an oxygen atmosphere at different temperatures. The surface and thickness of the films were evaluated by scanning electron microscopy (SEM). The structural property of the films was characterized by X-ray diffractometer (XRD) ( $\text{Cu-K}\alpha$  radiation,  $\lambda = 0.154$  nm). The elemental composition and chemical state were investigated by X-ray photoelectron spectroscopy (XPS).

The MSM  $\text{Ga}_2\text{O}_3$  photodetectors were fabricated by using the standard photolithography and lift-off techniques (see Fig. S1). We

used the semiconductor analyzer (Agilent B1500A) to measure the current–voltage ( $I-V$ ) property and the time-dependent photocurrent at room temperature. The spectral response property of the photodetectors was obtained by using a 150 W UV enhanced Xe lamp with a monochromator. The transient response spectra of the photodetectors were recorded by using an oscilloscope (Tektronix DPO 5104 digital oscilloscope) and a Nd:YAG laser (250 nm).

## 3. Results and discussion

**Fig. 1** shows the top-view and cross-sectional scanning electron microscopy (SEM) images of the as-grown and the post-annealed  $\text{a-Ga}_2\text{O}_3$  thin films. It can be seen that all the samples have the flat and smooth surface, which is further confirmed by the AFM images of the as-grown and the post-annealed  $\text{a-Ga}_2\text{O}_3$  thin films (as shown in Fig. S2). From the SEM images of **Fig. 1** and AFM images of **Fig. S2**, it can be obtained that few particles can be found on the surface of as-grown  $\text{a-Ga}_2\text{O}_3$  film, and the number of particles would decrease after annealing. With increasing the annealing temperature, almost no change can be found in the thickness of all the  $\text{a-Ga}_2\text{O}_3$  films (around 90 nm), which should be associated with the higher density of the ALD grown films and the relatively lower annealing temperature. **Fig. 2(a)** shows the transmission spectra of the as-grown and oxygen annealed  $\text{a-Ga}_2\text{O}_3$  films on sapphire substrates. It is obvious that the annealed  $\text{Ga}_2\text{O}_3$  films under different temperatures have the similar light absorption property with the as-grown sample. All the samples showed the average transmittance over 95% in the visible region with sharp absorption edges at ~250 nm. In order to investigate the structural properties of the different  $\text{Ga}_2\text{O}_3$  films, the X-ray diffractometer (XRD) measurement was carried out for the  $\text{a-Ga}_2\text{O}_3$  films as shown in **Fig. 2(b)**. When the annealing temperature was below 500 °C, no signature peak can be observed for the annealed  $\text{Ga}_2\text{O}_3$  films besides the (0006) diffraction peak of the sapphire substrates, indicating the same amorphous nature with the as-grown sample. As the annealing temperature increased to 550 °C, the amorphous sample begins to crystallize (see **Fig. 2(b)**), and the diffraction peaks appeared at  $2\theta = 37.2^\circ$  and  $38.3^\circ$  can be assigned to the (401) and (–402) planes of monoclinic  $\beta\text{-Ga}_2\text{O}_3$  (JCPDS: 43–1012), respectively. When the annealing temperature reached 650 °C, the XRD result showed that the thin film had been transformed from amorphous phase into monoclinic  $\beta\text{-Ga}_2\text{O}_3$  structure (see **Fig. S3**).

In order to investigate the optoelectronic properties of  $\text{a-Ga}_2\text{O}_3$  with and without annealing, metal-semiconductor-metal (MSM) photodetectors were fabricated on these films. **Fig. 3(a)** presents a schematic diagram of the  $\text{Ga}_2\text{O}_3$  MSM photodetector. 25 pairs of Au (30 nm thick) interdigitated electrodes with 10  $\mu\text{m}$  in width and 500  $\mu\text{m}$  in length and 10  $\mu\text{m}$  in space were fabricated on the  $\text{a-Ga}_2\text{O}_3$  films using the standard photolithography and lift-off techniques. Au metal contacts were deposited by ion sputtering. **Fig. 3(b)** describes the  $I-V$  characteristic curves of the different  $\text{Ga}_2\text{O}_3$  photodetectors in the dark with the voltage sweeping from –15 V to 15 V in steps of 200 mV. As shown in **Fig. 3(b)**, the dark current of the annealed  $\text{Ga}_2\text{O}_3$  photodetectors was obviously smaller than that of as-grown  $\text{Ga}_2\text{O}_3$  photodetector, and the dark current of the photodetectors decreased slightly with increasing the annealing temperature, which may be associated with the reduction of oxygen vacancy defects in the  $\text{Ga}_2\text{O}_3$  films [38]. Notably, the  $I-V$  curve of as-grown and low-temperature-annealed  $\text{a-Ga}_2\text{O}_3$  photodetectors showed an obvious asymmetric behavior when the voltage was swept from –15 V to 15 V. This phenomenon was commonly observed in metal/ $\text{Ga}_2\text{O}_{3-x}$ /metal structure based on oxygen deficiency gallium oxide thin films [39,40], and thus the asymmetric  $I-V$  behavior of as-grown and low-temperature-annealed  $\text{a-Ga}_2\text{O}_3$  photodetectors should be related to the oxygen

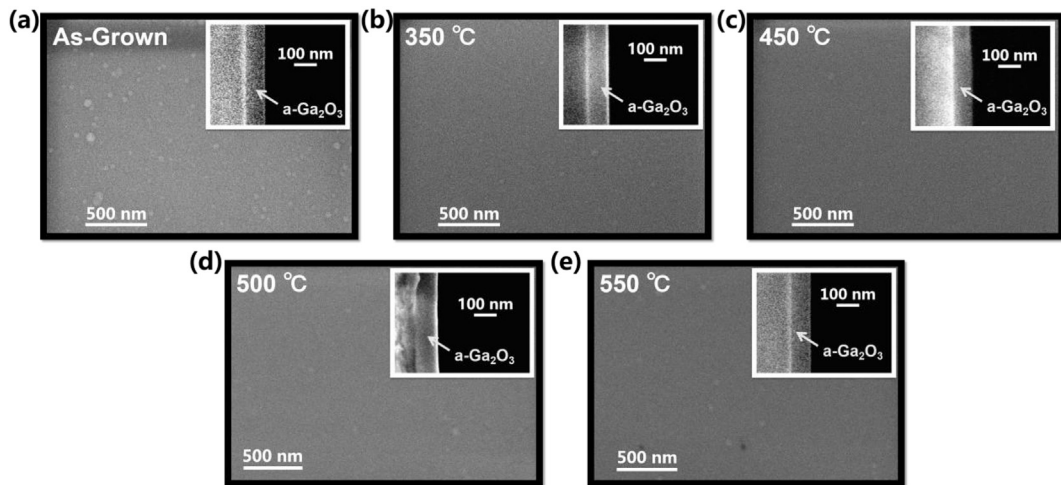


**Fig. 1.** Top-view and cross-sectional SEM images of the as-grown a-Ga<sub>2</sub>O<sub>3</sub> thin film (a) and the Ga<sub>2</sub>O<sub>3</sub> thin films annealed at 350 °C (b), 450 °C (c), 500 °C (d) and 550 °C (e).

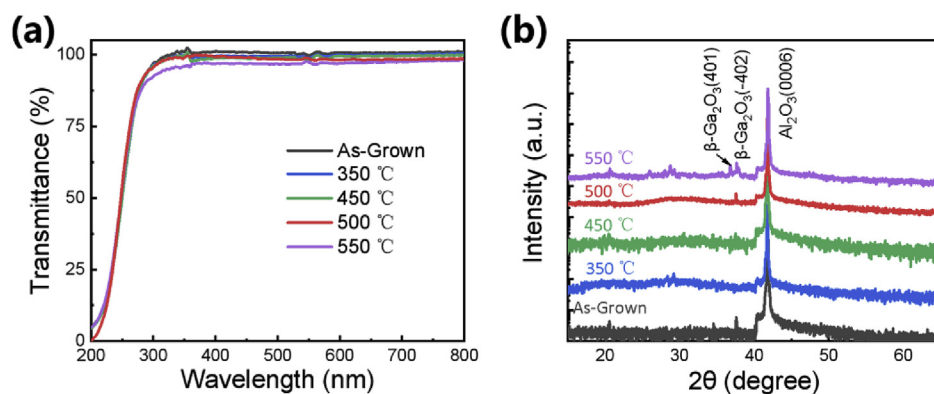


**Fig. 2.** (a) Transmission spectra and (b) XRD patterns of the Ga<sub>2</sub>O<sub>3</sub> films with and without annealing.

vacancy defect in the films. Fig. 3(c) gives the *I*–*V* curves of the photodetector under 254 nm UV light illumination. It can be clearly obtained that the photocurrent of the a-Ga<sub>2</sub>O<sub>3</sub> photodetectors decreased gradually with increasing the annealing temperature, and once the crystallization of a-Ga<sub>2</sub>O<sub>3</sub> occurred after 550 °C annealing, the photocurrent was significantly reduced.

The response properties of the a-Ga<sub>2</sub>O<sub>3</sub> photodetectors were measured by using a 150 W UV enhanced Xe lamp with a monochromator. Fig. 4(a) shows the spectral responses of the as-grown and annealed Ga<sub>2</sub>O<sub>3</sub> photodetectors under a bias of 10 V plotted on a logarithmic scale. The peak responses of the Ga<sub>2</sub>O<sub>3</sub> photodetectors occur at around 250 nm. After the annealing in oxygen at different temperatures, the responsivities of the photodetectors showed an obvious decrease. In particular, 500 °C annealing could decrease the responsivity from 28 A/W to 1.34 A/W. According to the previous reports, the oxygen vacancies in the absorbing layer could capture the excess photogenerated carriers, reducing the electron-hole recombination and in turn leading to a high responsivity [41,42]. Thus, the decrease in oxygen vacancies should be responsible for the reduction of photocurrent of the a-Ga<sub>2</sub>O<sub>3</sub> photodetectors after oxygen annealing. The rejection ratio ( $R_{250\text{nm}}/R_{400\text{nm}}$ ) of the a-Ga<sub>2</sub>O<sub>3</sub> photodetectors, which is defined as the ratio of the responsivity values at 250 nm and 400 nm, is only  $4.3 \times 10^3$  for the as-grown a-Ga<sub>2</sub>O<sub>3</sub> device. Interestingly, with the annealing temperature increasing, the rejection ratios were improved from 3 orders to 5 orders of magnitude due to the significant suppression

of the visible light response. Notably, the UV/Visible rejection ratio of the photodetector annealed at 500 °C is as high as  $2.74 \times 10^5$ , which is greater than any other previously reported a-Ga<sub>2</sub>O<sub>3</sub> photodetectors to the best of our knowledge. This phenomenon can be attributed to the decrease of oxygen vacancy defects, which usually cause the extrinsic transitions from the defect levels to the conduction band [27,30,43]. This excellent wavelength selectivity is helpful to highly sensitive solar-blind photodetection. The repeatability is also an important factor in determining the long-term stable dynamic operation of a photodetector. The time dependence of photocurrent property was measured at 10 V by switching ON/OFF 254 nm light with a power density of 1.39 mW/cm<sup>2</sup>. As presented in Fig. 4(b), all photodetectors demonstrated excellent reproducibility and stability during operation.

To further investigate the response speed of a-Ga<sub>2</sub>O<sub>3</sub> photodetectors, the transient response property was measured at 10 V by using a pulsed Nd:YAG laser with a wavelength of 250 nm (the laser pulse width was 10 ns, and the frequency was 10 Hz). The response time is defined as the time interval between the 10% and 90% of amplitudes. As shown in Fig. 5, the 10–90% rise times  $t_r$  for all photodetectors are around 10 ns, which should be limited by the laser pulse width. The 90–10% decay times  $t_d$  decrease gradually with increasing the annealing temperature, and it can reach as short as 140 ns after 550 °C annealing. In order to better understand the effect of annealing temperature on a-Ga<sub>2</sub>O<sub>3</sub>, Table 1 summarizes the performance of all the Ga<sub>2</sub>O<sub>3</sub> detectors with and without

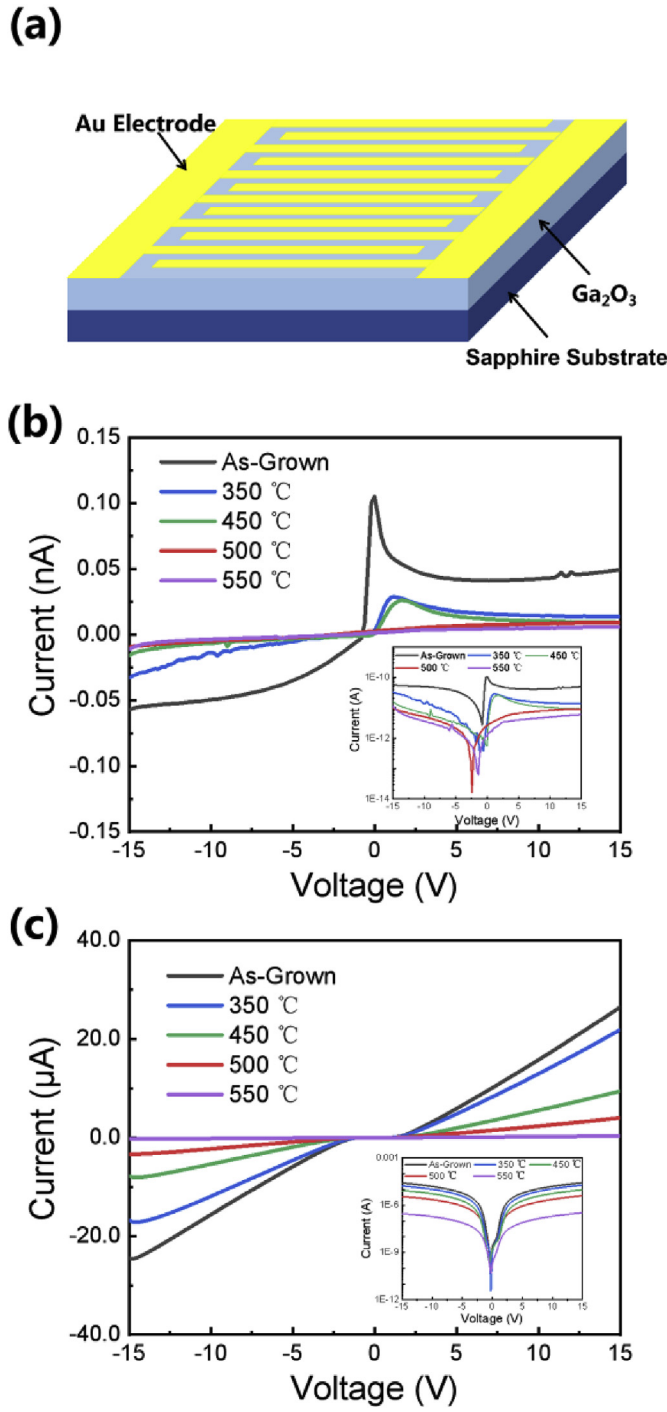


**Fig. 3.** (a) Schematic illustration of the photodetector. (b)  $I$ - $V$  curves of the photodetectors in the dark (b) and under UV 254 nm light illumination (c) (The inset is the  $I$ - $V$  curve with y scale setting to log).

oxygen annealing. It can be clearly found that the  $\text{Ga}_2\text{O}_3$  UV photodetector annealed at 500 °C has the best overall performance among the devices based on amorphous materials. Furthermore, Table 2 summarizes the performance parameters of our a- $\text{Ga}_2\text{O}_3$  photodetector annealed at 500 °C and the other recently reported photodetectors based on  $\text{Ga}_2\text{O}_3$  films [22–24,26–30,35,37,47,48]. It is clear that our  $\text{Ga}_2\text{O}_3$  photodetector has the fastest response speed ( $t_r = 10$  ns,  $t_d = 150$  ns) and the highest rejection ratio ( $2.74 \times 10^5$ ). The a- $\text{Ga}_2\text{O}_3$  photodetectors in this work exhibited an obvious

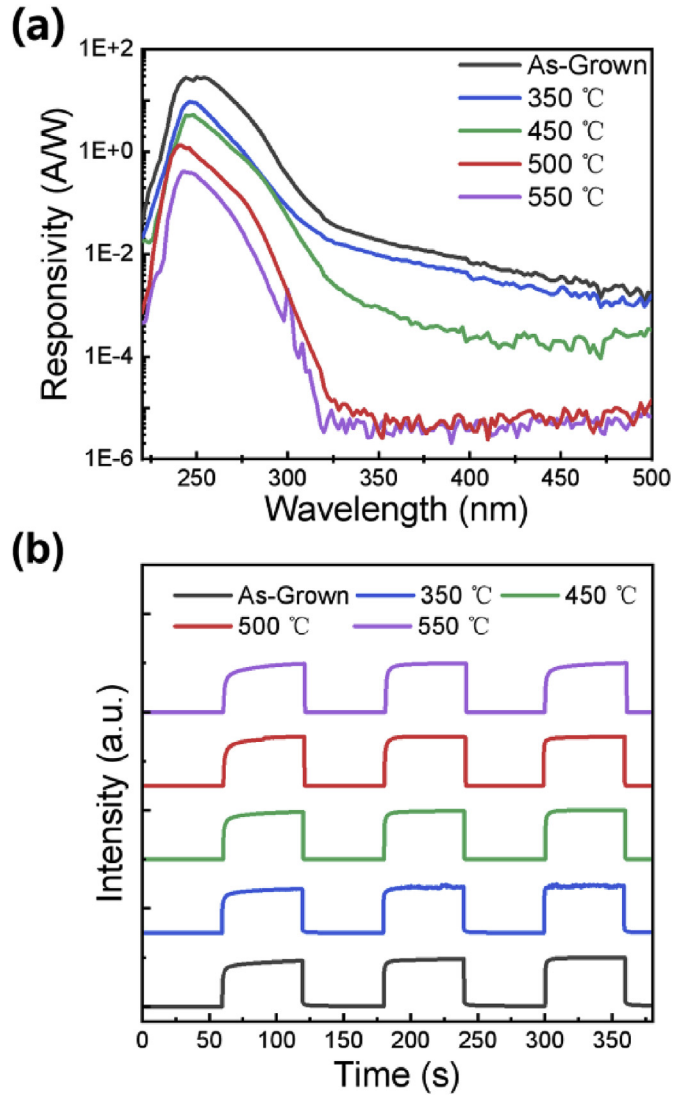


**Fig. 4.** (a) Photoresponsivity spectra of the photodetectors biased at 10 V. (b) Time-dependent photocurrent of the photodetectors at 10 V under 254 nm light illumination.

improvement in the photoresponse speed and the rejection ratio after the annealing in oxygen atmosphere. To further explain the detailed mechanism of the abovementioned phenomenon, the X-ray photoelectron spectroscopy (XPS) measurement has been carried out on the as-grown and annealed a- $\text{Ga}_2\text{O}_3$  films. In order to avoid the influence of oxygen adsorption on the film surface, sample surface was etched before recording the XPS data. Fig. 6 describes the O1s XPS spectra of the a- $\text{Ga}_2\text{O}_3$  films with and without annealing. Each O1s spectrum could be deconvoluted into two components based on Gaussian fitting analysis: one peak ( $\text{O}_{\text{I}}$ ) is at around 530.5 eV from the contribution of O–Ga bonds of  $\text{Ga}_2\text{O}_3$  and another one ( $\text{O}_{\text{II}}$ ) at around 531.2 eV can be attributed to the  $\text{O}^{2-}$  ions in the oxygen-deficient regions [37,44–46]. We can see that the  $\text{O}_{\text{II}}$  peak is highly suppressed after annealing under the oxygen atmosphere. In addition, the intensity ratio of  $\text{O}_{\text{II}}/(\text{O}_{\text{I}} + \text{O}_{\text{II}})$  which reflects the densities of oxygen vacancies were calculated to be 46%, 41%, 39%, 38% and 35% for the as-grown, 350 °C-, 450 °C-, 500 °C- and 550 °C-annealed  $\text{Ga}_2\text{O}_3$  films, respectively. And we also calculated the O/Ga ratio of different  $\text{Ga}_2\text{O}_3$  films. According to the O1s and  $\text{Ga}2\text{p}_{3/2}$  peak intensities, the O/Ga ratios of the all a- $\text{Ga}_2\text{O}_3$

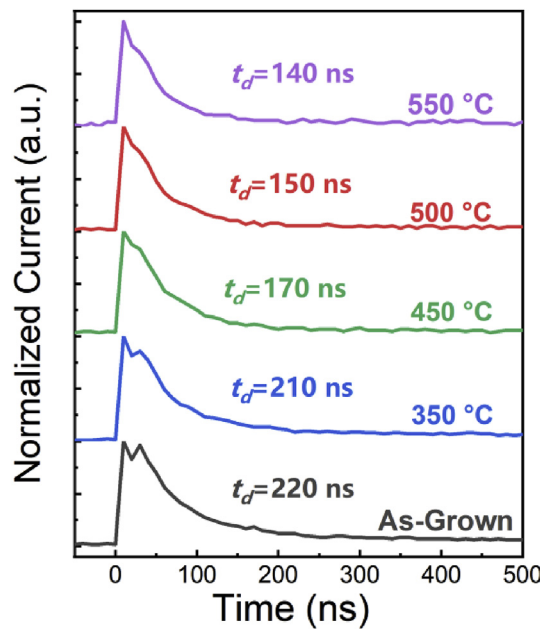


**Fig. 5.** Transient photoresponse of photodetectors at 10 V under the illumination of a 250 nm pulsed laser.

films were estimated to be 0.20, 0.23, 0.24, 0.27 and 0.29 for the as-grown, 350 °C-, 450 °C-, 500 °C- and 550 °C-annealed Ga<sub>2</sub>O<sub>3</sub> films, respectively. From the XPS result, it is suggested that the oxygen vacancy concentration obviously decreased with increasing the annealing temperature under the oxygen atmosphere. Generally, oxygen vacancy defects in the Ga<sub>2</sub>O<sub>3</sub> films could act as electron traps that reduce the electron-hole recombination and in turn

could help in effective photodetection. Meanwhile, the trapping effect of oxygen vacancy would increase the response time. Additionally, the additional visible light absorption related to the oxygen vacancy defect levels could cause the photoresponse in the visible region, decreasing the UV/Visible rejection ratio. Therefore, the oxygen annealing on the a-Ga<sub>2</sub>O<sub>3</sub> films can enhance the rejection ratio and the response speed of the detectors with a decrease in responsivity. To further confirm the mechanism of the performance enhancement of Ga<sub>2</sub>O<sub>3</sub> photodetector by oxygen annealing, the a-Ga<sub>2</sub>O<sub>3</sub> films were annealed under Ar atmosphere and their photodetectors have also been realized and investigated. After annealing in Ar at 500 °C, no obvious change can be found in the XRD, transmission spectrum and O1s XPS spectrum for a-Ga<sub>2</sub>O<sub>3</sub> (see Fig. S4). Meanwhile, both the dark current and the responsivity were decreased slightly, and the UV/Visible rejection ratio showed no big change (see Fig. S5). By comparing the performance of Ga<sub>2</sub>O<sub>3</sub> photodetectors annealed under Ar and O<sub>2</sub> atmospheres at 500 °C, it can be confirmed that the performance enhancement of the detector annealed under O<sub>2</sub> atmosphere is related to the reduction of oxygen vacancies in the film.

#### 4. Conclusions

In summary, solar-blind UV photodetectors with fast-speed and high-rejection-ratio were fabricated on a-Ga<sub>2</sub>O<sub>3</sub> film by ALD. The effect of the post-annealing under oxygen atmosphere on the performance of a-Ga<sub>2</sub>O<sub>3</sub> photodetectors has been investigated. With the increase of the annealing temperature, the response speed and the rejection ratio of the photodetectors increased obviously. After the oxygen annealing at 500 °C, the 90–10% decay time and the rejection ratio of a-Ga<sub>2</sub>O<sub>3</sub> photodetector were respectively around 150 ns and 2.74×10<sup>5</sup>, which are much better than that of the any previously reported a-Ga<sub>2</sub>O<sub>3</sub> based photodetectors. And the XPS results suggested that the decrease of oxygen

**Table 1**  
The performance parameters of all the 550 °C crystalline and the amorphous Ga<sub>2</sub>O<sub>3</sub> photodetectors at 10 V.

Annealing temperature	Dark current (pA)	Responsivity (A/W)	90–10% decay time (ns)	Rejection ratio
As-Grown	43.6	28	220	4.3×10 <sup>3</sup>
350 °C	17.2	9.5	210	2.6×10 <sup>3</sup>
450 °C	14.6	5.37	170	2.34×10 <sup>4</sup>
500 °C	9.43	1.34	150	2.74×10 <sup>5</sup>
550 °C	0.26	0.405	140	1.10×10 <sup>5</sup>

**Table 2**  
The performance parameters of our a-Ga<sub>2</sub>O<sub>3</sub> photodetector annealed at 500 °C and the other recently reported photodetectors based on Ga<sub>2</sub>O<sub>3</sub> films.

Detector	Method	Film thickness/electrode spacing	Dark current (pA)	Responsivity (A/W)	90–10% decay time (s)	Rejection ratio	Ref.
a-Ga <sub>2</sub> O <sub>3</sub> (500 °C annealing in O <sub>2</sub> )	ALD	90 nm/10 μm	9.43@10 V	1.34@10 V	150×10 <sup>-9</sup>	2.74×10 <sup>5</sup>	This work
a-Ga <sub>2</sub> O <sub>3</sub>	magnetron sputtering	125 nm/5 μm	16.3×10 <sup>6</sup>	55.5@5 V	769.4×10 <sup>-6</sup>	10	26
a-Ga <sub>2</sub> O <sub>3</sub>	magnetron sputtering	–/–	338.6@10 V	76.26@10 V	0.02	1.15×10 <sup>5</sup>	27
a-Ga <sub>2</sub> O <sub>3</sub>	ALD	30 nm/30 μm	200@10 V	45.11@20 V	148×10 <sup>-6</sup>	–	28
a-Ga <sub>2</sub> O <sub>3</sub>	magnetron sputtering	250 nm/2 μm	–	0.19@10 V	19.1×10 <sup>-6</sup>	–	29
a-Ga <sub>2</sub> O <sub>3</sub>	magnetron sputtering	–/5 μm	4040@10 V	–	0.3	10 <sup>4</sup>	30
β-Ga <sub>2</sub> O <sub>3</sub>	LMBE	200 nm/200 μm	1.28×10 <sup>5</sup>	–	1.02/16.61	–	22
β-Ga <sub>2</sub> O <sub>3</sub>	MOCVD	–/100 μm	–	0.07	–	–	23
β-Ga <sub>2</sub> O <sub>3</sub>	PLD	220 nm/100 μm	12@5 V	0.903@5 V	–	7867	24
β-Ga <sub>2</sub> O <sub>3</sub>	RFMS	318 nm/100 μm	110@10 V	–	0.05/0.92	10 <sup>3</sup>	35
β-Ga <sub>2</sub> O <sub>3</sub>	LMBE	–/100 μm	5×10 <sup>4</sup>	–	0.83/8.14	–	37
α-Ga <sub>2</sub> O <sub>3</sub>	LMBE	–/200 μm	1200	0.015@20 V	–	–	47
α-Ga <sub>2</sub> O <sub>3</sub>	ALD	30 nm/–	0.5@10 V	0.76@20 V	89×10 <sup>-6</sup>	10 <sup>4</sup>	48

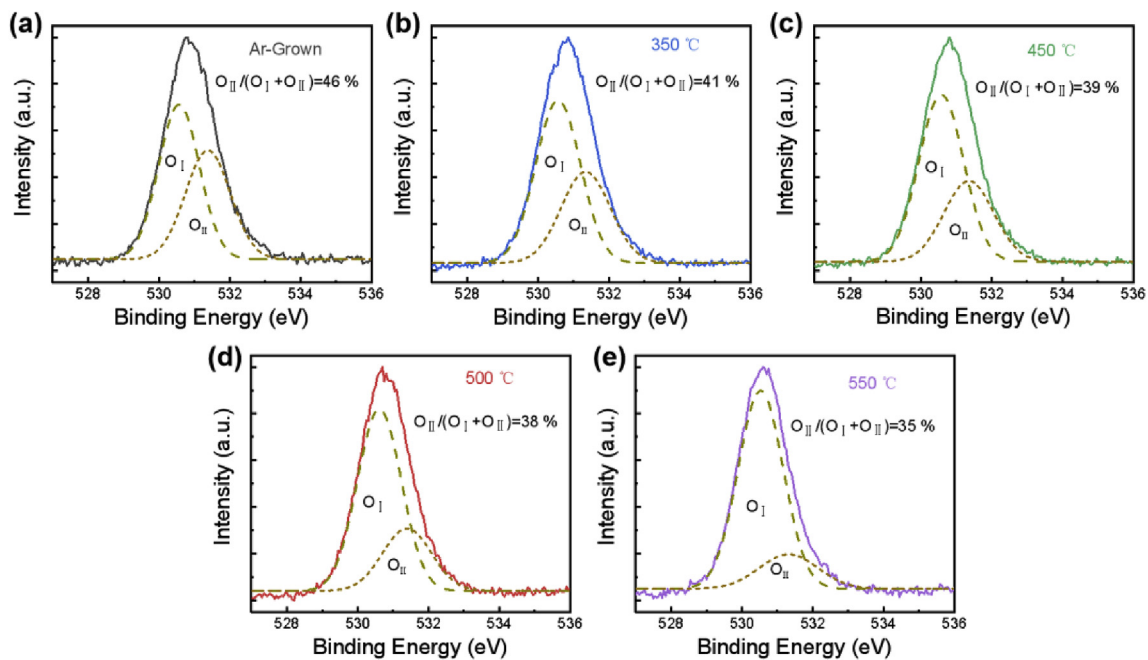


**Fig. 6.** O1s XPS spectra of the as-grown (a), 350 °C-annealed (b), 450 °C-annealed (c), 500 °C-annealed (d) and 550 °C-annealed (e)  $\text{Ga}_2\text{O}_3$ .

vacancy concentration should be responsible for the response speed and the rejection ratio improvement of the annealed a- $\text{Ga}_2\text{O}_3$  photodetectors. The findings in this work provide a viable way to realize the high-performance a- $\text{Ga}_2\text{O}_3$  solar-blind UV detectors.

#### Declaration of competing interest

The authors declare that they have no known competing financial interests or personal relationships that could have appeared to influence the work reported in this paper.

#### CRediT authorship contribution statement

**Changqi Zhou:** Conceptualization, Data curation, Formal analysis, Investigation, Methodology, Writing - original draft. **Kewei Liu:** Validation, Formal analysis, Writing - review & editing, Supervision, Resources. **Xing Chen:** Resources, Supervision. **Jiaheng Feng:** Supervision, Methodology. **Jialin Yang:** Supervision, Methodology. **Zhenzhong Zhang:** Resources, Supervision. **Lei Liu:** Resources, Supervision. **Yang Xia:** Supervision. **Dezhen Shen:** Writing - review & editing, Supervision, Resources.

#### Acknowledgment

This work is supported by the National Natural Science Foundation of China (61475153, 61605200, 61875194, 11727902, 61425021, 61525404, 61427901), Jilin Province Young and Middle-aged Science and Technology Innovation Leaders and Team Project (20180519023JH), the 100 Talents Program of the Chinese Academy of Sciences, Jilin Province Science Fund for Excellent Young Scholars (20180520173JH), Open Project of the State Key Laboratory of Luminescence and Applications (SKLA-2018-05).

#### Appendix A. Supplementary data

Supplementary data to this article can be found online at <https://doi.org/10.1016/j.jallcom.2020.155585>.

#### References

- [1] M. Razeghi, A. Rogalski, Semiconductor ultraviolet detectors, *J. Appl. Phys.* 79 (1996) 7433–7473.
- [2] Z. Alaie, S. Mohammad Nejad, M. Yousefi, Recent advances in ultraviolet photodetectors, *Mater. Sci. Semicond. Process.* 29 (2015) 16–55.
- [3] H. Chen, K. Liu, L. Hu, A. Al-Ghamdi, X. Fang, New concept ultraviolet photodetectors, *Mater. Today* 18 (2015) 493–502.
- [4] H. Chen, P. Yu, Z. Zhang, F. Teng, L. Zheng, K. Hu, X. Fang, Ultrasensitive self-powered solar-blind deep-ultraviolet photodetector based on all-solid-state Polyaniline/MgZnO bilayer, *Small* 12 (2016) 5809–5816.
- [5] X. Xu, J. Chen, S. Cai, Z. Long, Y. Zhang, L. Su, S. He, C. Tang, P. Liu, H. Peng, X. Fang, A real-time wearable UV-radiation monitor based on a high-performance p-CuZnS/n-TiO<sub>2</sub> photodetector, *Adv. Mater.* 30 (2018) 1803165.
- [6] W. Ouyang, F. Teng, X. Fang, High performance BiOCl nanosheets/TiO<sub>2</sub> nanotube arrays heterojunction UV photodetector: the influences of self-induced inner electric fields in the BiOCl nanosheets, *Adv. Funct. Mater.* 28 (2018) 1707178.
- [7] K. Hu, F. Teng, L. Zheng, P. Yu, Z. Zhang, H. Chen, X. Fang, Binary response Se/ZnO p-n heterojunction UV photodetector with high on/off ratio and fast speed, *Laser Photon. Rev.* 11 (2017) 1600257.
- [8] F. Foulon, P. Bergonzo, C. Borel, R. Marshall, C. Jany, L. Besombes, A. Brambilla, D. Riedel, L. Museur, M. Castex, A. Gicquel, Solar blind chemically vapor deposited diamond detectors for vacuum ultraviolet pulsed light-source characterization, *J. Appl. Phys.* 84 (1998) 5331–5336.
- [9] E. Cicek, R. McClintock, C. Cho, B. Rahmema, M. Razeghi,  $\text{Al}_x\text{Ga}_{1-x}\text{N}$ -based back-illuminated solar-blind photodetectors with external quantum efficiency of 89%, *Appl. Phys. Lett.* 103 (2013) 191108.
- [10] M. Fan, K. Liu, X. Chen, X. Wang, Z. Zhang, B. Li, D. Shen, Mechanism of excellent photoelectric characteristics in mixed-phase ZnMgO ultraviolet photodetectors with single cutoff wavelength, *ACS Appl. Mater. Interfaces* 7 (2015) 20600–20606.
- [11] W. Kong, G. Wu, K. Wang, T. Zhang, Y. Zou, D. Wang, L. Luo, Graphene-beta- $\text{Ga}_2\text{O}_3$  heterojunction for highly sensitive deep UV photodetector application, *Adv. Mater.* 28 (2016) 10725–10731.
- [12] R. Suzuki, S. Nakagomi, Y. Kokubun, Solar-blind photodiodes composed of a Au Schottky contact and a  $\beta$ - $\text{Ga}_2\text{O}_3$  single crystal with a high resistivity cap layer, *Appl. Phys. Lett.* 98 (2011) 131114.
- [13] S. Lim, Y. Ko, C. Rodriguez, S. Gong, Y. Cho, Electrically driven, phosphor-free, white light-emitting diodes using gallium nitride-based double concentric truncated pyramid structures, *Light Sci. Appl.* 5 (2016), e16030.
- [14] Y. Kokubun, K. Miura, F. Endo, S. Nakagomi, Sol-gel prepared  $\beta$ - $\text{Ga}_2\text{O}_3$  thin films for ultraviolet photodetectors, *Appl. Phys. Lett.* 90 (2007), 031912.
- [15] J. Xu, W. Zheng, F. Huang, Gallium oxide solar-blind ultraviolet photodetectors: a review, *J. Mater. Chem. C* 7 (2019) 8753–8770.
- [16] B. Zhao, F. Wang, H. Chen, L. Zheng, L. Su, D. Zhao, X. Fang, An ultrahigh responsivity (9.7 mA/W) self-powered solar-blind photodetector based on individual ZnO- $\text{Ga}_2\text{O}_3$  heterostructures, *Adv. Funct. Mater.* 27 (2017) 1700264.

- [17] J. Yu, Z. Nie, L. Dong, L. Yuan, D. Li, Y. Huang, L. Zhang, Y. Zhang, R. Jia, Influence of annealing temperature on structure and photoelectrical performance of  $\beta$ -Ga<sub>2</sub>O<sub>3</sub>/4H-SiC heterojunction photodetectors, *J. Alloys Compd.* 798 (2019) 458–466.
- [18] X. Zhang, L. Wang, X. Wang, Y. Chen, Q. Shao, G. Wu, X. Wang, T. Lin, H. Shen, J. Wang, X. Meng, J. Chu, High-performance  $\beta$ -Ga<sub>2</sub>O<sub>3</sub> thickness dependent solar blind photodetector, *Optic Express* 8 (2020) 1089–1109.
- [19] H. Li, S. Yuan, T. Huang, H. Chen, F. Lu, S. Zhang, D. Wuu, Impact of thermal-induced sapphire substrate erosion on material and photodetector characteristics of sputtered Ga<sub>2</sub>O<sub>3</sub> films, *J. Alloys Compd.* 823 (2020) 153755.
- [20] Hao Shen, Karthikeyan Baskaran, Yinong Yin, Kun Tian, Libing Duan, Xiaoru Zhao, Ashutosh Tiwari, Effect of thickness on the performance of solar blind photodetectors fabricated using PLD grown  $\beta$ -Ga<sub>2</sub>O<sub>3</sub> thin films, *J. Alloys Compd.* 822 (2020) 153419.
- [21] J. Yu, L. Dong, B. Peng, L. Yuan, Y. Huang, L. Zhang, Y. Zhang, R. Jia, Self-powered photodetectors based on  $\beta$ -Ga<sub>2</sub>O<sub>3</sub>/4H-SiC heterojunction with ultrahigh current on/off ratio and fast response, *J. Alloys Compd.* 821 (2020) 153532.
- [22] D. Guo, Z. Wu, P. Li, Y. An, H. Liu, X. Guo, H. Yan, G. Wang, C. Sun, L. Li, W. Tang, Fabrication of  $\beta$ -Ga<sub>2</sub>O<sub>3</sub> thin films and solar-blind photodetectors by laser MBE technology, *Opt. Mater. Express* 4 (2014) 1067.
- [23] C. Huang, R. Horng, D. Wuu, L. Tu, H. Kao, Thermal annealing effect on material characterizations of  $\beta$ -Ga<sub>2</sub>O<sub>3</sub> epilayer grown by metal organic chemical vapor deposition, *Appl. Phys. Lett.* 102 (2013), 011119.
- [24] F. Yu, S. Ou, D. Wuu, Pulsed laser deposition of gallium oxide films for high performance solar-blind photodetectors, *Opt. Mater. Express* 5 (2015) 1240.
- [25] B. Qiao, Z. Zhang, X. Xie, B. Li, K. Li, X. Chen, H. Zhao, K. Liu, L. Liu, D. Shen, Avalanche gain in metal–semiconductor–metal Ga<sub>2</sub>O<sub>3</sub> solar-blind photodiodes, *J. Phys. Chem. C* 123 (2019) 18516–18520.
- [26] Y. Zhang, X. Chen, Y. Xu, F. Ren, S. Gu, R. Zhang, Y. Zheng, J. Ye, Transition of photoconductive and photovoltaic operation modes in amorphous Ga<sub>2</sub>O<sub>3</sub>-based solar-blind detectors tuned by oxygen vacancies, *Chin. Phys. B* 28 (2019), 028501.
- [27] L. Qian, Z. Wu, Y. Zhang, P. Lai, X. Liu, Y. Li, Ultrahigh-responsivity, rapid-recovery, solar-blind photodetector based on highly nonstoichiometric amorphous gallium oxide, *ACS Photonics* 4 (2017) 2203–2211.
- [28] S. Lee, S. Kim, Y. Moon, S. Kim, H. Jung, M. Seo, K. Lee, S. Kim, S.W. Lee, High-responsivity deep-ultraviolet-selective photodetectors using ultrathin gallium oxide films, *ACS Photonics* 4 (2017) 2937–2943.
- [29] S. Cui, Z. Mei, Y. Zhang, H. Liang, X. Du, Room-temperature fabricated amorphous Ga<sub>2</sub>O<sub>3</sub> high-response-speed solar-blind photodetector on rigid and flexible substrates, *Adv. Opt. Mater.* 5 (2017) 1700454.
- [30] H. Liang, S. Cui, R. Su, P. Guan, Y. He, L. Yang, L. Chen, Y. Zhang, Z. Mei, X. Du, Flexible X-ray detectors based on amorphous Ga<sub>2</sub>O<sub>3</sub> thin films, *ACS Photonics* 6 (2019) 351–359.
- [31] H. Zhou, L. Cong, J. Ma, B. Li, M. Chen, H. Xu, Y. Liu, High gain broadband photoconductor based on amorphous Ga<sub>2</sub>O<sub>3</sub> and suppression of persistent photoconductivity, *J. Mater. Chem. C* 7 (2019) 13149.
- [32] S. Han, X. Huang, M. Fang, W. Zhao, S. Xu, D. Zhu, W. Xu, M. Fang, W. Liu, P. Cao, Y. Lu, High-performance UV detectors based on room-temperature deposited amorphous Ga<sub>2</sub>O<sub>3</sub> thin films by RF magnetron sputtering, *J. Mater. Chem. C* 7 (2019) 11834.
- [33] W. Zhu, L. Xiong, J. Si, Z. Hu, X. Gao, L. Long, T. Li, R. Wan, L. Zhang, L. Wang, Influence of deposition temperature on amorphous Ga<sub>2</sub>O<sub>3</sub> solar-blind ultraviolet photodetector, *Semicond. Sci. Technol.* 35 (2020), 055037.
- [34] D. Guo, X. Qin, M. Lv, H. Shi, Y. Su, G. Yao, S. Wang, C. Li, P. Li, W. Tang, Decrease of oxygen vacancy by Zn-doped for improving solar-blind photoelectric performance in  $\beta$ -Ga<sub>2</sub>O<sub>3</sub> thin films, *Electron. Mater. Lett.* 13 (2017) 483–488.
- [35] J. Wang, L. Ye, X. Wang, H. Zhang, L. Li, C. Kong, W. Li, High transmittance  $\beta$ -Ga<sub>2</sub>O<sub>3</sub> thin films deposited by magnetron sputtering and post-annealing for solar-blind ultraviolet photodetector, *J. Alloys Compd.* 803 (2019) 9–15.
- [36] X. Liu, P. Guo, T. Sheng, L. Qian, W. Zhang, Y. Li,  $\beta$ -Ga<sub>2</sub>O<sub>3</sub> thin films on sapphire pre-seeded by homo-self-templated buffer layer for solar-blind UV photodetector, *Opt. Mater.* 51 (2016) 203–207.
- [37] D. Guo, Z. Wu, Y. An, X. Guo, X. Chu, C. Sun, L. Li, P. Li, W. Tang, Oxygen vacancy tuned Ohmic–Schottky conversion for enhanced performance in  $\beta$ -Ga<sub>2</sub>O<sub>3</sub> solar-blind ultraviolet photodetectors, *Appl. Phys. Lett.* 105 (2014), 023507.
- [38] M. Heinemann, J. Berry, G. Teeter, T. Unold, D. Ginley, Oxygen deficiency and Sn doping of amorphous Ga<sub>2</sub>O<sub>3</sub>, *Appl. Phys. Lett.* 108 (2016), 022107.
- [39] X. Gao, Y. Xia, J. Ji, H. Xu, Y. Su, H. Li, C. Yang, H. Guo, J. Yin, Z. Liu, Effect of top electrode materials on bipolar resistive switching behavior of gallium oxide films, *Appl. Phys. Lett.* 97 (2010) 193501.
- [40] D. Guo, Z. Wu, Y. An, P. Li, P. Wang, X. Chu, X. Guo, Y. Zhi, M. Lei, L. Li, W. Tang, Unipolar resistive switching behavior of amorphous gallium oxide thin films for nonvolatile memory applications, *Appl. Phys. Lett.* 106 (2015), 042105.
- [41] J. Liu, C. Shan, B. Li, Z. Zhang, C. Yang, D. Shen, X. Fan, High responsivity ultraviolet photodetector realized via a carrier-trapping process, *Appl. Phys. Lett.* 97 (2010) 251102.
- [42] O. Katz, V. Garber, B. Meyler, G. Bahir, J. Salzman, Gain mechanism in GaN Schottky ultraviolet detectors, *Appl. Phys. Lett.* 79 (2001) 1417–1419.
- [43] J. Jang, J. Park, B. Ahn, D. Kim, S. Choi, H. Kim, D. Kim, Study on the photoresponse of amorphous In-Ga-Zn-O and zinc oxynitride semiconductor devices by the extraction of sub-gap-state distribution and device simulation, *ACS Appl. Mater. Interfaces* 7 (2015) 15570–15577.
- [44] Y. An, D. Guo, S. Li, Z. Wu, Y. Huang, P. Li, L. Li, W. Tang, Influence of oxygen vacancies on the photoresponse of  $\beta$ -Ga<sub>2</sub>O<sub>3</sub>/SiC n–n type heterojunctions, *J. Phys. D Appl. Phys.* 49 (2016) 285111.
- [45] Y. Liao, S. Jiao, S. Li, J. Wang, D. Wang, S. Gao, Q. Yu, H. Li, Effect of deposition pressure on the structural and optical properties of Ga<sub>2</sub>O<sub>3</sub> films obtained by thermal post-crystallization, *CrystEngComm* 20 (2018) 133–139.
- [46] S. Park, T. Ikegami, K. Ebihara, Effects of substrate temperature on the properties of Ga-doped ZnO by pulsed laser deposition, *Thin Solid Films* 513 (2006) 90–94.
- [47] D. Guo, X. Zhao, Y. Zhi, W. Cui, Y. Huang, Y. An, P. Li, Z. Wu, W. Tang, Epitaxial growth and solar-blind photoelectric properties of corundum-structured  $\alpha$ -Ga<sub>2</sub>O<sub>3</sub> thin films, *Mater. Lett.* 164 (2016) 364–367.
- [48] S. Lee, K. Lee, Y. Kim, Y. Moon, S. Kim, D. Bae, T. Kim, Y. Kim, S. Kim, S. Lee, Sub-microsecond response time deep-ultraviolet photodetectors using  $\alpha$ -Ga<sub>2</sub>O<sub>3</sub> thin films grown via low-temperature atomic layer deposition, *J. Alloys Compd.* 780 (2019) 400–407.